Chapter 1

Introduction

"Begin with the end in Mind."

- Stephen Covey, The 7 habits of highly effective people

In this chapter, we begin with an overview of radio surveys. We discuss the role of low frequency surveys in radio astronomy and briefly describe a few important surveys. With this background we describe the MRT survey followed by a brief description of the Mauritius Radio Telescope (MRT). An outline of this dissertation is given at the end of this chapter.

1.1 Radio surveys : An overview

The science of radio astronomy began with the observations of the radio sky at low frequencies. The pioneering discovery of cosmic radio emission was made at 20.5 MHz by Karl Jansky in 1931 (Jansky, 1932). The first systematic survey of the radio universe was carried out by Grote Reber in 1940 (Reber, 1944) at 160 MHz with a resolution of 12°. It revealed that radio signals come from many directions in the sky, predominantly from the constellations of Cygnus, Cassiopeia, Canis Major, Pupis etc., apart from the Galactic center and the Sun. It also revealed that the nature of this radiation is non-thermal. Since then, surveying the radio sky and compiling catalogues of radio sources have been an important part of astronomical research. Surveys have led to many astronomical discoveries and in fact to much of modern astrophysics. A large fraction of famous objects studied by radio astronomers like radio galaxies, quasars, BL Lac objects, pulsars and gravitational lenses were discovered in early surveys.

Surveys are intended to give a global view of the sky. The sources in a typical radio survey may include radio galaxies, radio loud AGNs (Active Galactic Nuclei), quasars, BL Lac objects, star burst galaxies, radio stars, diffuse cluster emission, radio halos of nearby galaxies, relic radio sources, compact sources, planetary nebulae, supernova remnants (SNRs), pulsars etc.. The distribution of extragalactic radio sources in the sky is almost isotropic because the mean separation between two extragalactic radio sources is more than 10 Mpc, which is the galaxy clustering correlation length. This isotropic nature is one of the strongest evidence that galaxies obey cosmological evolution and the matter distribution is homogeneous on large scales in the universe (Condon, 1999; Peebles, 2002). Sources emit radio waves by one or more of several processes like thermal radiation from solid bodies such as planets and stars, thermal bremsstrahlung radiation from hot gas in the interstellar medium, synchrotron radiation from relativistic electrons in magnetic fields, spectral radiation from atomic and molecular transitions that occur in the interstellar medium or in gaseous envelopes around stars, pulsed radiation resulting from the rapid rotation of neutron stars surrounded by an intense magnetic field and energetic electrons. New class of sources in radio surveys can open qualitatively different and

exciting new scientific applications from which we learn new astrophysics.

One of the primary goals of surveys is to produce flux density limited samples of large regions of the celestial sky. Many scientific studies need complete samples above some flux density (mJy) but all surveys produce images which are brightness limited (mJy beam^{-1}). This distinction can be generally safely ignored for large scale surveys in which most of the extragalactic sources are unresolved. Low luminosity sources such as normal galaxies (like NGC 2442), in which the radio emission is located within the visible extent of the galaxy and tends to be stronger in regions of star formation, are not detectable at large distances because of their low luminosity and hence form only a small fraction of most of the radio samples. In a flux density limited sample, most of the radio sources are extragalactic and evolution dominates their redshift distribution at all flux density (S) cutoffs $S < 10$ Jy (at ν=1.4 GHz). The cosmological evolution of extragalactic radio sources is so strong at all observed luminosities that the local luminosity function and counts of all sources between $S \approx 10\,\mu$Jy and $S \approx 10$ Jy at ν=1.4 GHz can be matched with a model in which most of the sources are confined to a hollow shell with a median redshift of $\approx$1 (Condon (1998) and references therein). In other words, the median redshift of all the sources fainter than about 10 Jy is $\approx$1, nearly independent of the flux density. This implies that *deep radio surveys do not probe further into the universe, they only find intrinsically fainter sources*. Even early radio surveys with poor sensitivity could detect distant galaxies and discover objects like quasars, BL lacs and demonstrated that the universe evolves with time. Unfortunately very few radio sources are close enough to be studied easily in other wavelength ranges (like optical), on account of which most of the radio sources have never been identified with known individual objects.

Surveys enable construction of complete samples of source populations. For any survey it is desirable to have nearly uniform sensitivity across the sky for generating large source samples. This gives a more reliable overall view of the sky and a more homogeneous sample. Using their statistical properties one can study/infer cosmological evolution. The unbiased and homogeneous samples from the surveys help in testing models and rejecting those which may work only on a few peculiar astronomical sources. In addition, it provides a list of sources and interesting regions of the sky which can be chosen for further studies depending upon the scientific objectives in mind. An example of the most famous and well studied complete sample is the 3CRR sample (Laing et. al., 1983).

One of the important aspects of a survey is that it promotes multi-wavelength studies. The scientific aims and returns of a large radio survey is enormously increased if the optical counterparts are identified, the optical spectra classified and the redshifts measured. The estimation of redshift helps us to calculate the intrinsic properties of radio

galaxies like their physical size, radio luminosity, energy density, pressure, magnetic field etc.. In an ideal situation, if one knows the characteristic redshift distribution of all the radio sources in a large sensitive survey as a function of flux density, one can measure the evolution of radio luminosity function with redshift and also study the three dimensional clustering of radio sources. In practice this is difficult to achieve but one expects significant progress in near future with the use of ongoing large area multicolor optical, infrared and near infrared imaging surveys (like SDSS[1], 2MASS[2],2dFGRS[3]) which will measure the photometric redshifts down to faint optical galaxies. Cross-matching radio source surveys with the optical redshift surveys may provide redshift and spectroscopic data for a large number of galaxies. One example of a study which reveals the potential of combining low frequency data with an optical redshift survey is by Sadler et. al. (2001). AGNs have either pure absorption line spectrum like that of a giant elliptical galaxy or a stellar continuum plus nebular emission lines of OII and OIII which are strong compared to any Balmer like emission. Star forming galaxies have strong narrow emission lines of H_α and usually H_β. Sadler et. al. (2001) cross matched the NVSS[4] radio catalogue with the first thirty fields (100 deg^2) observed in the 2dF Galaxy Redshift Survey (Colless et. al., 1999) and found that it is straightforward to tell from the optical spectra whether the radio emission arose from the star formation or AGN. This distinction is helpful in classifying the chief cause of radio emission. Similarly, radio loud X-ray sources can be found by cross matching the radio sources with X-Ray surveys like ROSAT[5] all sky survey (Voges et. al., 1999). Generally such radio sources having X-ray counterparts are quasars. Radio surveys are ideal tools to study the evolution of active and star forming galaxies from the local to the distant universe. Radio-Far Infrared (FIR) correlation is an important tool for identification of star forming galaxies.

Radio surveys have also been used to disentangle the superposition of sources along complex lines of sight. This is done using the contrast between non-thermal emitters and free-free absorbing HII regions. Such a study applied to HII regions in and around W30 SNR complex (Kassim & Weiler, 1990), helped in placing Sgr A west in front of the non-thermal Sgr A east (Pedlar et. al., 1989).

[1]Sloan Digital Sky Survey ; http://www.sdss.org
[2]Two Micron All Sky Survey ; http://www.ipac.caltech.edu/2mass
[3]2dF Galaxy Redshift Survey ; http://www.mso.anu.edu.au/2dFGRS, http://magnum.anu.edu.au/~TDFgg
[4]NRAO VLA Sky Survey; http://www.cv.nrao.edu/nvss
[5]http://wave.xray.mpe.mpg.de/rosat

1.2 Role of low frequency surveys in radio astronomy

The radio window covers several decades in frequency. Surveys at different frequencies select different source populations. Over many years, low frequency surveys ($15 \leq \nu \leq 500$ MHz) have played a very important role in Astronomy and Astrophysics. Apart from the general use of any survey (Sec. 1.1), there are other benefits of a low frequency survey.

The most prominent mechanism of emission in most of the radio sources is the synchrotron radiation. For a homogeneous and isotropic ensemble of electrons accelerated in the presence of a magnetic field, the observed flux density (S) due to synchrotron radiation approximates to a power law (Ginzburg & Syrovatskii, 1969; Moffet, 1975).

$$S \propto \nu^{-\alpha}$$

where α is the spectral index and ν is the observing frequency. The spectral index[6] depends upon the energy spectrum of the electrons and is given by,

$$\alpha \sim (\gamma - 1)/2$$

where γ is a parameter which depends upon the distribution of electrons in the energy spectrum,

$$N(E)\,dE \propto E^{-\gamma} dE$$

where E is the energy and $N(E)$ is the number density of the electrons in the energy spectrum. Generally the spectral index of radio sources in the frequency range 0.1 GHz-1 GHz is around 0.5-1.0.

Low frequency favors the study of non-thermal sources which are generally brighter at low frequencies. Sources selected at low frequencies are dominated by unbeamed emission and give an unbiased view of their parent population. This is used by unification models to account for diversity of sources seen at high frequencies (Wall & Jackson, 1997). Low frequency images enable measurement of the continuum spectra which traces the underlying electron energy distribution of incoherent synchrotron emission for studies of shock acceleration and spectral aging in galactic (like SNRs) and extragalactic (like radio galaxies) sources. Low frequency surveys favor sources with exceptionally steep spectra (α >1.2), which could likely be high redshift radio galaxies, quasars or millisecond pulsars. Large scale diffuse structures such as radio relics, lobes, plumes and bridges are due to old electrons and hence are more prominent at low frequencies. Coherent emission from the Sun, Earth, Jupiter, extra-solar planets etc. occur primarily at low frequencies (Erickson, 1999).

[6]Spectral index α between two frequencies ν_1 and ν_2 is given by $\alpha_{\nu_1}^{\nu_2} = -\frac{log(S_2/S_1)}{log(\nu_2/\nu_1)}$.

Studies of the high redshift objects are important in understanding galaxy formation and links with nuclear activity (Spinrad, 1986). These are generally characterized by their steep spectrum and small angular size. These two features are extensively used in filtering the sample of sources in low frequency radio surveys as potential candidates for high redshift galaxies (Rawlings et. al., 1996; De Breuck et. al., 2000, 2004; Van Breugel et. al., 1999) and has been the most efficient and successful method (Chambers et. al., 1996a,b). Most of the high redshift radio galaxies known so far including the most distant ones, have been detected using these searches.

About 10% of the powerful radio galaxies produce directed radio jets which transport a vast supply of energy for as long as 10^8-10^9 years over distances up to a few Mpc to the synchrotron emitting lobes also known as Gaint Radio Galaxies (GRG) (Kassim et. al., 2002). These represent probably the last stages of radio galaxy evolution and provide unique probes of the intergalactic medium. Their luminosities can be as high as 10^{28} W Hz^{-1} Sr^{-1} due to which they can be detected at great distances even with moderate sensitivity. The detection of a large number of such high redshift objects is important for our understanding of the origin of active galaxies. At high redshifts the universe is young and this leaves little time for jet-producing central engines and host galaxies to form. Above 1 GHz, radio galaxy lobes are subject to synchrotron losses. In addition, their lobes suffer from inverse compton losses, due to scatterring of the cosmic microwave background radiation whose energy density increases as $(1+z)^4$. Since an observing frequency ν_{obs}, samples a galaxy at a redshift of z at the rest frame frequency $(1+z)\nu_{obs}$, it is important to observe them at low observing frequencies. The advantage of using these steep spectrum high redshift radio galaxies and quasars as beacons of the distant universe is that the radio emission does not suffer from dust obscuration. Low frequency surveys which are sensitive to large angular size and low surface brightness are well suited for detection of these GRGs.

De Breuck et. al. (1998) have also recently discovered a new class of ultra-steep-spectrum, highly polarized, red, dusty quasar WN J0717+4611 at z=1.462. Low-frequency observations would be an efficient means of finding additional objects of this nature. Pulsars were discovered at low frequency (Hewish et. al., 1968). Since millisecond pulsars are characterized by steep spectrum, compact steep spectrum sources are excellent candidates for searching them.

Synchrotron aging of a relativistic electron population preferentially depletes the high energy electrons first. Low energy electrons which radiate at low radio frequencies have longest lifetimes. The population of electrons whose radiation lifetimes exceed the Hubble age suggests the existence of extremely steep spectrum fossil galaxies. It has been suggested that the cluster radio relics in the vicinity of clusters of galaxies are in fact such fossil

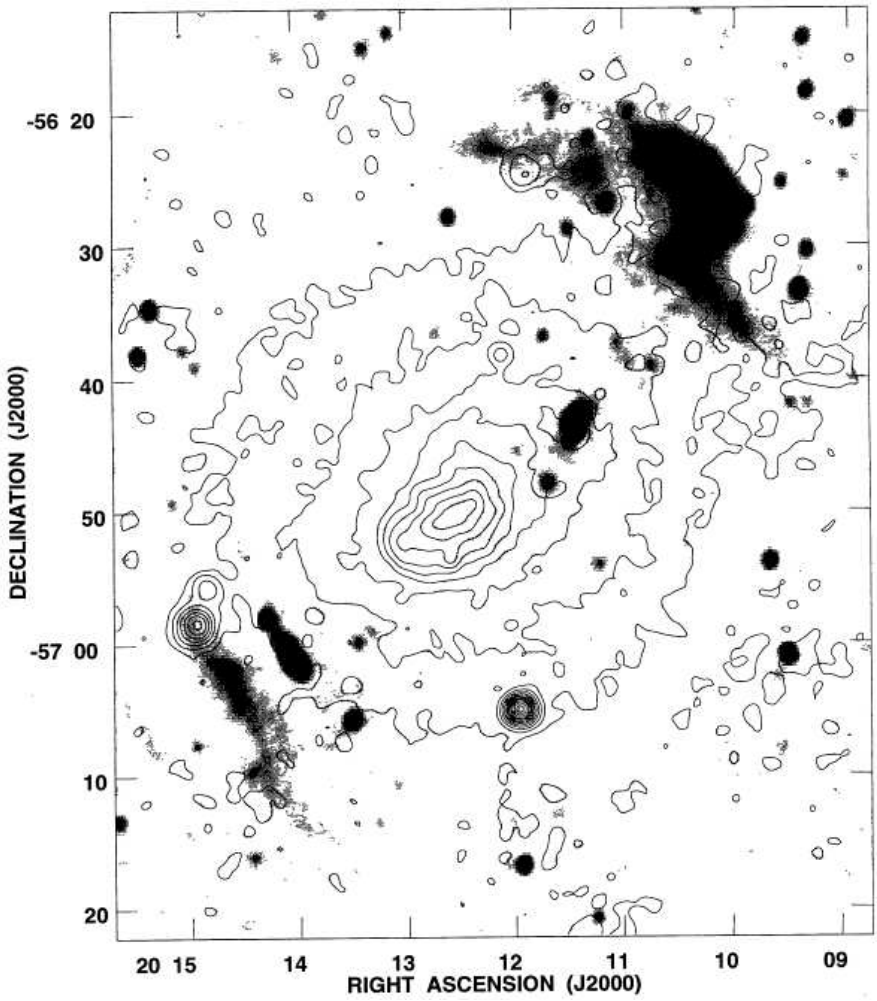

Fig. 1.1: Image of the region around the cluster Abell 3667. It shows a contour representation of the ROSAT PSPC image (0.1-2 Kev), overlaid on a gray scale radio image at 843 MHz from the MOST. The X-ray contours are set at 2, 8, 18, 32, 50, 72, 98, 128, 162, 200 and 242 $\times$ the background noise. The steep spectrum halo radio emission is believed to be due to the shocks formed between in-falling matter and the cluster core. (Courtesy Röttgering et. al. (1997))

galaxies, with shock accelerated relativistic electron population (Ensslin & Bierman, 1998). The necessary shock waves would be of Mpc scale and could be due to steady accretion of matter onto the cluster or due to a merger event with another cluster. Recently observed substructures in X-ray temperature maps support the existence of extended shock waves at locations of several known cluster relics (Markevitch et. al., 1998; Donelly et. al., 1998). Fig. 1.1 shows such an example of these proposed shocks around the X-ray cluster Abell 3667; both (thermal) X-ray emission from the cluster core and 843 MHz radio emission from the shock accelerated electron population in the presumed in-falling matter shocks, are visible (Röttgering et. al., 1997). These reactivated fossil galaxies are powerful tools to investigate the properties of in-falling matter onto the clusters of galaxies and

a test ground of large scale structure formation. They are steep spectrum sources, so low frequency observations would be helpful to detect more such sources.

Radio halos are diffuse, central radio emission regions in galaxy clusters and do not seem to be associated with any one galaxy in the cluster. It is believed that they have steep spectrum due to which they often escape detection at higher frequencies. Low frequency survey favors detection and study of such interesting sources. Synchrotron radio halos have been predicted around all types of individual galaxies but have rarely been reliably detected (Kronberg, 1990). Low frequency observations are critical because they are excellent tracers of large scale structure and the physics of underlying radiation losses suffered by the transported electrons is revealed through the slope of the spectral index gradients.

SNRs are extended non-thermal emitting sources and are the principal sources of energy input to the Inter Stellar Medium (ISM). Often their large angular sizes are well matched to the large fields of view easily available at low frequencies, for studying and detection of new candidates. Useful information can be gained from the morphology and integrated low frequency spectra of the SNRs which helps in their classification. An excellent example is the image at 330 MHz which was used to discover the second closest known SNR to the Galactic center (Kassim et. al., 1998; Kassim & Frail, 1996). The low frequency spectra has been successfully used to distinguish between HII regions and SNRs. Predictions from the Fermi-acceleration theory imply concave integrated spectra i.e. hardening at higher frequencies. Sensitive low frequency surveys may lead to discovery of older, low surface brightness SNRs which are known to be missing from catalogues due to severe selection effects. Discovery of such old SNRs at the last stage of their evolution before blending into the ISM are potentially of great importance in discovering new pulsar-SNR associations and drawing links to unidentified γ-ray sources.

Low frequency observations offer unique insights into the interaction of thermal and non-thermal processes and self absorption processes. A variety of absorption processes are expected to occur in and around radio galaxies at low frequencies. These include synchrotron self absorption, Razin-Tsytovich suppression, turnovers caused by low-energy cutoffs in electron energies and absorption by thermal gas. In normal galaxies such as M82, Wills et. al. (1997) detected a larger free-free absorption of SNRs by giant HII regions at 151 MHz and 408 MHz than that towards Galactic SNRs (Kassim, 1989). Such measurements place constraints on the radial location of the discrete non-thermal sources, relative to the ionized component of the ISM of the host galaxy. Also on larger scales the integrated spectra of many normal galaxies appear to flatten near 100 MHz. This flattening may be due to free-free absorption by the cool ISM gas.

Low frequency observations are capable of distinguishing between

intrinsic (synchrotron self absorption, source variability) and extrinsic (free-free absorption scattering) physical processes affecting the non-thermal emission at low frequencies. Physical parameters of the ISM - cosmic ray emissivity, emission measure, temperature, pressure and ionization state can be constrained from low frequency observations of HII regions and recombination lines from very high Rydberg state atoms. Below frequencies around 100 MHz, HII regions may become opaque thereby providing walls at known distances to allow distance estimates to various foreground objects in our galaxy and external galaxies.

Using their low frequency image of the radio galaxy Virgo A and comparing them with the X-ray images, Owen & Eilek (1999) showed that the large scale halo is a response to the activity of the Virgo A black hole jet system, contrary to the conventional belief that it is a relatively young feature. Similar studies of low frequency images may substantially change our understanding of astronomical objects.

1.3 Renewed interest in low frequency surveying

Carrying out large scale survey at low frequencies has its own interesting peculiarities. The field of view, primary beam solid angle $\Omega_b \propto \lambda^2$ is large, so the number of fields required to map the sky, $4\pi/\Omega_b$ is much smaller. This makes gridded low frequency surveys more efficient for surveying. This large coverage is needed to yield useful number of nearby sources or rare interesting sources like steep spectrum sources. This is also desirable for statistical work since the sampling error decreases as the size of the sample increases.

The sensitivity of a low frequency survey is generally determined by confusion noise[7] due to faint unresolved sources in the synthesized beam. Due to this at low frequencies, the resolution is also crucial in determining the depth of the survey. High resolution which is difficult to obtain at low frequencies is also required for detailed information about the structure of the object and measuring accurate positions. Positional accuracy of a source is useful while cross matching it with other surveys and especially for optical identification. In addition at low frequencies wide primary beam sidelobes of far away strong sources often limit the achieved dynamic range. In order to achieve good surface brightness sensitivity to detect extended sources, good *uv* coverage including the low spatial frequencies is needed.

Early radio surveys were made at decametre wavelengths with low resolution and sensitivity. Due to the difficulty in construction and maintenance of large arrays which are

[7]Confusion noise : There is a flux density below which there is more than one unresolved source per synthesized beam. These weaker sources are not perceptible individually, but the statistical fluctuations in their number present in each beam cause an apparent increase of noise.

essential to get high resolution, surveying soon shifted to higher frequencies once the high frequency receivers were available. Inspite of this difficulty, a few low frequency surveys were carried out. From these surveys came both serendipitous discoveries and the catalogues of sources used for high resolution mapping at higher frequencies. Table 1.1 gives important specifications of a few important low frequency surveys.

In addition to lack of high resolution and sensitivity, severe corruption due to Radio Frequency Interference (RFI) and ionospheric phase distortions limiting the array size have been some difficult aspects of low frequency astronomy. The wide field of view requires 3-D inversion and deconvolution with a varying Point Spread Function (PSF) both demanding intense computation. Due to these natural difficulties, the low frequency spectrum of radio astronomy remains poorly explored region of the electromagnetic spectrum despite immense scientific potential. In fact there are a number of important astrophysical questions which can be answered only by low frequency observations (like direct detection of epoch of reionization signal) in addition to those which may be more usefully addressed by observations over a wider range of frequencies.

Due to the advancement of technology especially in electronics and high speed computation, the scenario for low frequency imaging has changed. Field of view calibration and self calibration techniques to remove the ionospheric distortions over long baselines has made high resolution imaging possible at low frequencies which are least affected by confusion. In addition, due to the need for multi-wavelength studies, interest in low frequency astronomy has been revived. This scenario promises exciting time for astrophysics using low frequency astronomy.

A wide range of surveys have been recently undertaken or planned. They include 74 MHz VLA[8] Low-frequency Sky Survey (VLSS) (Cohen et. al., 2004), 325 MHz Westerbork Northern Sky Survey (WENSS) (Rengelink et. al., 1997), 843 MHz Sydney University Molonglo Sky Survey (SUMSS)(Bock et. al., 1999; Mauch et. al., 2003), 1.4 GHz NRAO VLA Sky Survey (NVSS) (Condon, 1998), 1.4 GHz Faint Images of the Radio Sky at Twenty-cm (FIRST) (Becker et. al., 1995; White et. al., 1997) etc.. Various new telescopes capable of imaging at low frequencies have been proposed or are under construction like Expanded Very Large Array (EVLA), Long Wavelength Array (LWA[9]), eXtended New Technology Demonstrator (XNTD[10]) (using Focal Plane Arrays), Mileura Wide-field Array (MWA[11]), Low Frequency Array (LOFAR[12]) and a next generation ground based international tele-

[8]Very Large Array
[9]http://lwa.unm.edu
[10]http://www.atnf.csiro.au/projects/ska/xntd.html
[11]http://web.haystack.mit.edu/arrays/MWA
[12]http://www.lofar.org

scope with very ambitious aims, the Square Kilometre Array (SKA[13]). All these have been possible with the help of recent innovative technological developments in both computing and radio frequency devices. SKA will be the world's premier imaging and surveying telescope with a combination of unprecedented versatility and sensitivity that will open up new windows for discovery. Now we describe a few important low frequency surveys keeping in mind their relevance to MRT survey.

1.4 A few important low frequency surveys

In this section, we look at some aspects of a few important low frequency radio surveys. Table 1.1 gives their specifications. It clearly indicates that there is no survey covering the southern sky in the frequency range 74 MHz (VLSS) to 352 MHz (WENSS). The VLSS and the WENSS cover the southern sky only north of δ=-30° and δ=-26° respectively. On the other hand, in the northern sky there are quite a few surveys around 150 MHz notably the 6C (Baldwin et. al., 1985; Hales et. al., 1988, 1990, 1991, 1993a,b), 3C/3CR (Edge et. al., 1959; Bennett, 1962) and the 4C (Pilkington & Scott, 1965; Gower et. al., 2001). Amongst these the 6C is by far the most extensive survey. This survey provides a moderately deep radio catalogue reaching a source density of about 2×10^4 sr^{-1} over most of the sky north of declination (δ), +30° with an angular resolution of $4\farcm2\times4\farcm2\,\csc(\delta)$ and a limiting flux density of about 120 mJy at 151 MHz.

Since MRT was designed with 6C survey in mind, we mention a few aspects related to it. The 6C survey has resulted in many important astronomical discoveries. One of them is the discovery of the galaxy NGC 6251 (Waggett et. al., 1977) with an angular size of $1\fdg2$ and a projected size of ≈3 Mpc when the survey was in its initial stages. Fig. 1.2 shows the contour image of the galaxy from the 6C survey. At the time of discovery, this galaxy was the largest angular source in the northern sky and was the second largest object in terms of projected size after 3C236. NGC6251 has a remarkable jet which is straight for nearly 200 Kpc. The radio spectral index of the jet is 0.54 and the nucleus has a flat spectrum with a cut off at low frequency. The cross section of the outer parts of the jet showed that the emission is distributed throughout the volume of the jet rather than in a thin walled cone containing it, as might be the case if a hypothetical beam supplying the energy to the outer components were to interact with the surrounding medium. The survey has also been successfully used for detection of high redshift galaxies (Blundell et. al., 1998) like 6C1232+39, 6C0901+35, 6C0930+38 (Rawlings et. al., 1990), including the detection of one of the most distant galaxies 6C0140+326 at a redshift of 4.41 (Rawlings et.

[13] http://www.skatelescope.org

Northern declination surveys					
Frequency (MHz)	Observatory	Resolution	Declination Coverage	Sensitivity	Number of Sources
34.5	GEETEE[a]	26′×42′	-30° to +60°	15 Jy	≈3000
38	Cambr. WKB[b]	45′× 45′	-45° to +35°	14 Jy	1000
74	VLSS[c]	80″×80″	-30° to +90°	500 mJy	ongoing
151	Cambr. 6C[d]	4′× 4′	+30° to +90°	120 mJy	≈35,000
178	Cambr. 3CR[e]	2′×2′	-5° to +90°	9 Jy	328
178	Cambr. 4C[f]	7.′5× 7.′5	-7° to +80°	2 Jy	4843
232	MSRT[g]	3.′8× 3.′8	30° to +90°	150 mJy	≈34,000
325	Westerbork[h]	54″ × 54″	29°to 90°	18 mJy	229,576
365	Texas[i]	10″ × 10″	-35.°7 to 71.°5	150 mJy	67,551
408	Effelsberg[j]	0.°85 × 0.°85	-10° to +50°	0.2 Jy	–
Southern declination surveys					
34.5	GEETEE	26′×42′	-30° to +60°	15 Jy	≈3000
38	Cambr. WKB	45′× 45′	-45° to +35°	14 Jy	1000
74	VLSS	80″×80″	-30° to +90°	500 mJy	ongoing
352	Westerbork	54″ × 54″	-26° to 9°	18 mJy	73,570
365	Texas	10″ × 10″	-35.°7 to 71.°5	150 mJy	67,551
408	Parkes[k]	0.°85×0.°85	-60° to +10°	1 Jy	–
408	Molonglo[l]	2′× 2′	-60° to +18°	0.6 Jy	>12000

Table 1.1: Surveys below 0.5 GHz. This is only a representative sample of the surveys available. The references are a-(Dwarakanath & Udaya Shankar, 1990), b-(Williams et. al., 1966), c-(Cohen et. al., 2004), d-(Baldwin et. al., 1985), e-(Bennett, 1962), f-(Pilkington & Scott, 1965; Gower et. al., 2001), g-(Zhang et. al., 1997), h-(Rengelink et. al., 1997), i-(Douglas et. al., 1996), j-(Haslam et. al., 1982), k-(Haslam et. al., 1975), l-(Large et. al., 1981).

al., 1996). The 6C survey has been successfully used to find GRGs and clusters (Saunders et. al., 1987). The survey has been used to study Radio-FIR (Far-InfraRed) correlation at lower frequencies. Far-infrared data from the IRAS survey was compared with 6C radio data at 151 MHz and a slope for the FIR/radio correlation of 0.86±0.03 was obtained. The slope of correlation between FIR and the low frequency radio luminosities is significantly different from unity in the sense that more luminous galaxies have a higher ratio of radio emission to FIR (Cox et. al., 1988). It revealed that radio emission at 151 MHz in radio sources is totally dominated by the non-thermal component which is mainly responsible for Radio-FIR correlation. One of the main conclusions of the study was that the low frequency radio emission is also strongly correlated with the FIR emission in star forming galaxies as in the case of high frequency emission. Models for the FIR emission from normal spiral galaxies were developed, showing that discrete SNRs cannot be responsible for the radio emission in either normal or starburst galaxies.

An equivalent of the 6C survey for the southern sky does not exist. Hence there is a need to survey the southern sky at low frequencies around 150 MHz. This existing lacuna of ra-

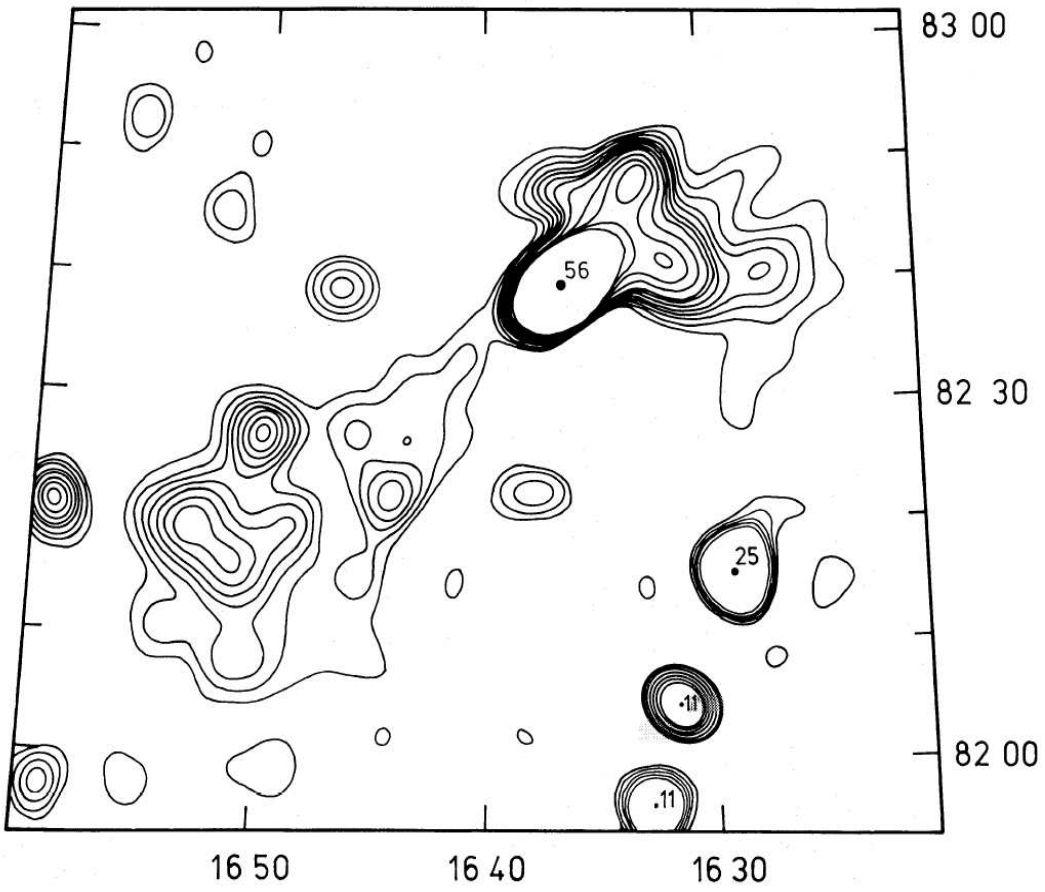

Fig. 1.2: Image of NGC6251 from 6C survey at 151 MHz. Beam size is 3.′7×3.′7. The contour interval is 70 mJy beam^{-1} (2σ). Peak values are given in units of contour interval. The coordinates are in B1950 epoch (courtesy Waggett et. al. (1977)).

dio surveys at low frequencies in the southern sky was the genesis of the MRT instrument. Its primary objective is to carry out MRT survey to map the southern sky at 151.5 MHz. The MRT survey covers all the sky in declination range -70° to -10° with a resolution (FWHM) 4′×4.′6 sec(δ+20.°14) and an expected point source sensitivity 330 mJy beam^{-1} (3σ).

The GEETEE survey (Dwarakanath & Udaya Shankar, 1990) is a wide-field continuum survey at 34.5 MHz. It covers the declination range of -30°$\leq \delta \leq$60°with a resolution of 26′×42′sec(δ-14.°1). The sensitivity is 5 Jy beam^{-1} (1σ) and is limited by confusion noise. It covers nearly the entire Galactic plane and special care was taken to ensure that the antenna responds to all angular scale structures and is suitable for studies of both point sources and extended structures. It also provides the brightness temperature of the sky covered. A comparative study of strong sources in the MRT survey, especially the extended sources like SNRs, would be an interesting aspect to investigate.

The 408 MHz survey by Haslam et. al. (1982) has a resolution of 0.°85 was the first all sky continuum survey having a resolution better than 1°. It was carried out with filled dishes

and gives the brightness temperature of the full sky. This survey and GEETEE survey are the only two surveys which give brightness temperature of the sky. The MRT survey is also designed to provide the brightness temperature of the sky covered at 151.5 MHz.

The Molonglo Reference Catalogue (MRC) (Large et. al., 1981) at 408 MHz contains 12,141 sources and has a resolution of $2\farcm62\times2\farcm86\sec(\delta\text{-}35\fdg5)$. It covers the sky between -85°<δ<18$\fdg$5 (|b| >3°) with a limiting flux density of ≈670 mJy. The catalogue is virtually complete at 1 Jy. Its nearly complete overlap with the region covered by the MRT survey, nearby frequency, similar resolution and comparable sensitivity makes this survey very special to MRT. It has been extensively used to cross check the images at various stages of data processing and for comparative studies. A flux density limited MRC-1 Jy complete sample constructed using this catalogue is the largest and most well studied complete sample in the southern sky (McCarthy et. al., 96).

The VLA Low-frequency Sky Survey covers the sky north of δ=-30°with a resolution of 80″ and a point source sensitivity of ≈500 mJy beam^{-1}. The survey expects to detect ≈100 relatively rare sources such as normal radio galaxies (Condon et. al., 1991). About 100 pulsars, steep spectrum halos surrounding nearby radio galaxies, fossil or relic radio sources which are diffuse, steep spectrum sources not obviously identified in anyway are expected. The survey will also extend the radio spectra of known source population to 74 MHz where free-free absorption and synchrotron self absorption become increasingly important. Evidence for free-free absorption within the first two Galactic SNRs imaged by VLA at 74 MHz suggests VLSS would reveal more such cases. The overlap of this survey with MRT survey can be well exploited for multi-frequency analysis.

Now we describe the MRT survey and its important scientific aspects followed by a brief overview of the MRT array.

1.5 The MRT survey

1.5.1 Scientific objectives

As mentioned earlier, the basic objective of the survey is to map the southern sky at 151.5 MHz in the declination range -70° to -10°with an expected point source sensitivity of ≈330 mJy (3σ) and an angular resolution of $4'\times4\farcm6\sec(\delta\text{+}20\fdg14)$.

The frequency of this survey was also preferred to be around 150 MHz because synchrotron sources show up much better than at higher frequencies such as 408 MHz due to their spectra. In addition sources also show up better than at lower frequencies since the absorption due to interstellar dust is much lesser than at decametre wavelengths. At 151.5 MHz the mean Galactic background brightness of ≈300 K does not dominate the

system noise temperature as it would at lower frequencies (Baldwin et. al., 1985). At 178 MHz (4C survey) the contamination by beamed sources is only 10% (Wall & Jackson, 1997). Thus samples selected at 151.5 MHz would be virtually dominated by isotropic radio emission (contamination by beamed sources will be even lesser) and would provide an unbiased view of the parent populations used in unification models. So 151.5 MHz was chosen as some kind of an optimal frequency for the survey.

The principal products of the survey would include wide-field images covering all sky in the declination range -70° to -10°. A catalogue of unresolved and extended sources along with their flux densities estimated from the images would extend the spectra of the radio source population to 151.5 MHz. This catalogue can be used to produce flux density limited complete samples for further studies including multi-frequency analysis. Due to low frequency and surface brightness sensitivity, MRT is also suited for the study of extended extragalactic sources such as giant radio sources and relics. The survey is expected to detect several such sources. The survey is expected to yield good sample of steep spectrum sources which would be likely candidates for high redshift galaxies and pulsars.

Although wide field images of the southern part of the Galactic plane will form a part of the MRT survey as a natural outcome, mapping the Galactic plane at low frequencies can be identified as a separate scientific objective in its own right. The geographic location of MRT is such that the Galactic center transits near the zenith. MRT with its low frequency of operation, wide field imaging capability and nearly complete *uv* coverage is well suited to image the southern part of the Galactic plane which has not been explored with this sensitivity and resolution earlier at such frequencies. It would be useful for investigating extended features like SNRs which are objects of typical size ≈11′and surface brightness sensitivity $\approx 5\times10^{-21}$ $Wm^{-2}Hz^{-1}Sr^{-1}$ (at 1 GHz). Morphology and non-thermal emission are primary signatures used for identification of SNRs in the Galaxy. Due to their large size and non-thermal nature, images for the survey would be useful to study their morphology, spectra and distinguish them from thermal sources like HII regions.

Fig. 1.3 shows the sensitivity and angular resolution as a function of frequency for most of the past and present low frequency imaging instruments in the 10-200 MHz range. In terms of expected sensitivity, MRT is less sensitive compared to 6C and VLSS, both of which primarily cover the northern sky. In terms of angular resolution MRT has less resolution compared to VLSS which covers southern sky only north of δ=-30° and is also at a different frequency. Culgoora catalogue has a slightly better resolution but it has been primarily used for spectral index measurements of known sources rather than a general survey. The comparison clearly reveals that MRT survey would play an important role at low frequencies.

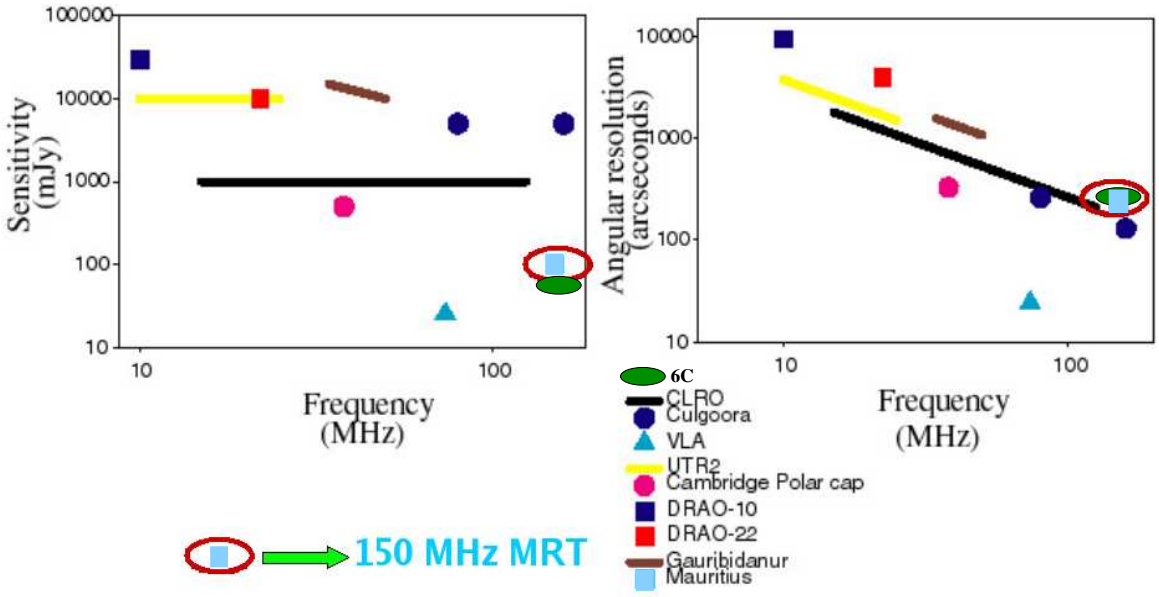

Fig. 1.3: Comparison of the sensitivity and angular resolution of MRT as a function of frequency with most of the past and present low frequency imaging instruments in the 10-200 MHz range (courtesy NRAO Summer School 2002, Namir Kassim). The 6C survey has been added by us to the original plot later.

Apart from carrying out the survey MRT has also been used for other studies. A survey with partial resolution of 17′×23′covering the RA range 18:00 hrs to 24:00 hrs and 00:00 hrs to 05:00 hrs and the declination (δ) range -70° to -10°, with a sensitivity of $\approx$0.8 Jy beam^{-1} (1σ) has been made (Golap, 1998). The genesis of this partial resolution survey lies in its usefulness in studying large scale structures and development of techniques for imaging with a non-coplanar array like MRT while data was being collected with longer baselines for the full resolution. A source catalogue of nearly 900 radio sources has been prepared.

A group of known SNRs which are possibly associated with pulsars were selected as one of the interesting studies. The geographical location gives a view of inner part of the galaxy where most of these supernova-pulsar associations are expected. The associations are important as they can put a lower limit to the age of the SNR which is also related to the energy loss mechanism of the pulsar. The associations of G5.4-1.2 with PSR 1758-23, G8.7-0.1 with PSR 1800-21, G320.4-1.2 with PSR 1509-58, G343.1-2.3 with PSR 1706-43 were investigated. The study indicates that most of the SNRs studied are associated with the pulsars or the proposed associations can be maintained. More details can be found in Dodson (1997).

The MRT pulsar observing system was set-up in July 1996 and has been used to observe about 30 pulsars at 150 MHz. About 10 pulsars have been detected, including the

Frequency	151.5 MHz
Bandwidth	1 MHz
Sky coverage	00^h <RA≤24^h, -70°≤ δ ≤-10°
Synthesized beam width	$4' \times 4.'6 \sec(\delta + 20.^\circ 14)$
Point source sensitivity* (1σ)	≈110 mJy
Surface brightness sensitivity* (1σ)	$\approx 7 \times 10^{-22}$ $Wm^{-2}Hz^{-1}Sr^{-1}$
Typical image size	15°×15°
Polarization	Right circular (IEEE)
uv coverage	uniform and complete
Aperture synthesis	sidereal hour wise, meridian transit

Table 1.2: Characteristics of MRT images. * refers to expected values.

bright millisecond pulsar (MSP) J0437-4715. This is the only MSP observable at such a low frequency making its study specially interesting and more so that it has some apparently unusual properties. Some of main results obtained are on the MSP J0437-4715 and on the 'core-single' normal pulsars J1453-6413 and J1752-2806. More details can be found in Issur (2000, 2002,a,b); Issur & Deshpande (2004).

The MRT is presently being used for observations of the radio emission from the Sun. This is in collaboration with the Gauribidanur Radio Heliograph (operated by Indian Institute of Astrophysics (IIA)) observations of the solar corona (Ramesh et. al., 2005).

1.5.2 Specifications

The important specifications of MRT are given in Table 1.2. Now we discuss its sky coverage, point source sensitivity, surface brightness sensitivity, expected number of sources and limiting redshift of the survey.

Sky coverage : The sky coverage of MRT survey (Ω_{MRT}) is given by,

$$\Omega_{MRT} = \int\int \cos\delta \, d\delta d\phi = \int_0^{2\pi} \int_{\delta_1=-70\times\frac{\pi}{180}}^{\delta_2=-10\times\frac{\pi}{180}} \cos\delta \, d\delta d\phi = 2\pi \, (\sin\delta_2 - \sin\delta_1) \approx 4.8 \text{ Sr} \qquad (1.1)$$

where ϕ is sidereal hour (in radians) and δ is declination. The sky coverage of MRT survey for the entire RA range (0^h to 24^h), i.e. ϕ varies from 0 rad to 2π rad and declination range -70° to -10° is ≈4.8 steradian.

Point source sensitivity : The minimum detectable flux density[14], ΔS_{min} ($1\,\sigma$), from a point source depends upon the thermal noise ($\Delta S_{thermal}$) and the confusion noise (ΔS_{conf}). Since the thermal noise and the confusion noise add in quadrature the effective limiting point source sensitivity is given by,

[14] Flux density is measured in units of Watts per square metre per unit frequency bandwidth ($W\,m^{-2}\,Hz^{-1}$). It is a measure of power per unit bandwidth falling on a unit area normal to the direction of arrival.

$$\Delta S_{min} = \sqrt{(\Delta S^2_{thermal} + \Delta S^2_{conf})} \tag{1.2}$$

Now we estimate both the thermal and the confusion noise to estimate the minimum detectable point source sensitivity.

a. **Thermal noise**

The thermal noise using an array of N_b baselines and a correlation receiver, without taking into account the bandwidth decorrelation, is given by (Thompson, Moran, & Swenson, 86),

$$\Delta S_{thermal} = \frac{\sqrt{2}\ 2k_B \sqrt{T_{sys_{ew}} T_{sys_{ns}}}}{\eta_{eff}\ \sqrt{N_b} A_e\ \sqrt{\Delta\nu t}} \tag{1.3}$$

where k_B is the Boltzmann constant.

$T_{sys_{ew}}$ and $T_{sys_{ns}}$ are the system temperatures of an EW group and a NS group respectively.

η_{eff} is the efficiency factor of a digital correlator. For a 2-bit 3-level quantizations at Nyquist rate its value is 0.81 (Bower & Klinger, 1974).

A_e is the effective collecting area of an interferometer pair. For a correlation receiver, the effective area $A_e = 2\sqrt{A_{EW}A_{NS}}$, where A_{EW}=128 m^2 and A_{NS}=16 m^2 are the areas of the EW and the NS groups, the two antennas forming the interferometer pair.

$\Delta\nu$ is the bandwidth, 1 MHz and t is the integration time, 4 s.

Fig. 1.4(a) shows the expected variation of system temperature[15] of an EW group, a NS group and the interferometer formed by EW and a NS group (EW×NS) as a function of RA. The minimum system temperature for an EW group is ≈650 K at RA≈04 hrs while the maximum system temperature is ≈2500 K at RA≈17:45 hrs. The minimum system temperature for an NS group is ≈660 K at RA≈04 hrs while the maximum system temperature is ≈2200 K at RA≈17:40 hrs. For the interferometer formed by the EW and the NS group, the minimum system temperature is ≈660 K at RA≈04 hrs and maximum system temperature is ≈2300 K at RA≈17:45 hrs.

Substituting the required values in the Eqn. 1.3, the thermal noise can be estimated as a function of RA. The minimum thermal noise is ≈110 mJy at RA≈04 hrs while the maximum thermal noise is ≈380 mJy at RA≈17:45 hrs.

b. **Confusion noise**

[15] Obtained by convolving the 408 MHz all-sky image with the beams of the EW group and the NS group. A temperature spectral index, α_T ($T \propto \nu^{-\alpha_T}$) of 2.7 is assumed.

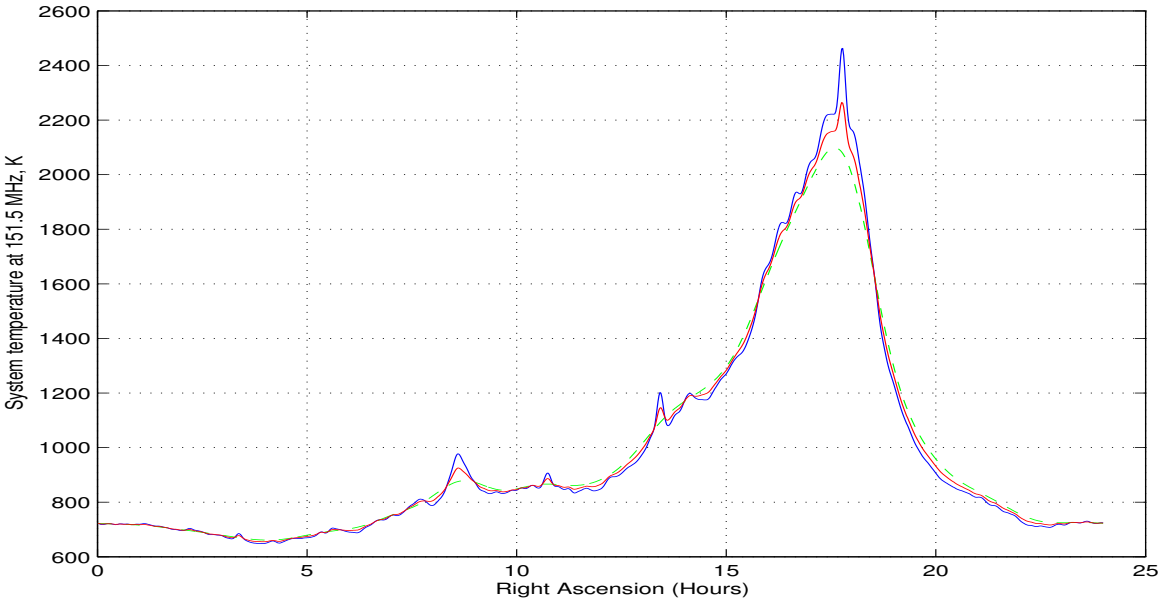

(a) The variation of system temperature as a function of RA of an EW group (blue solid line), a NS group (green dashed line) and the interferometer formed by EW and a NS group (EW×NS) (red solid line). The receiver temperature is assumed to be 400 K.

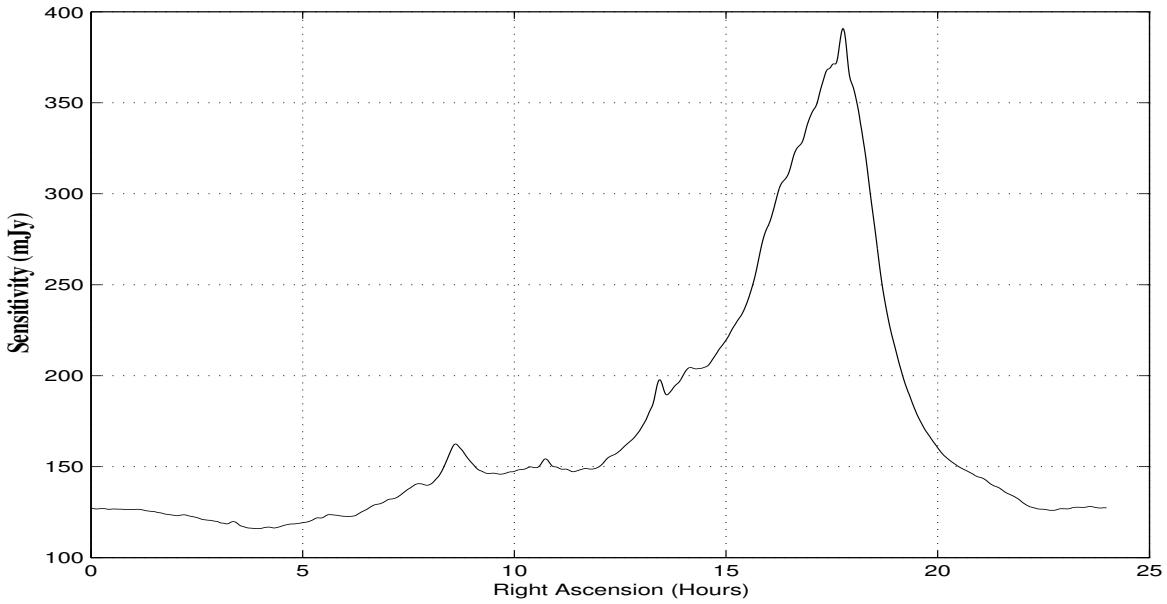

(b) Variation in sensitivity (mJy) as a function of RA for the survey (using all the allocations i.e. ≈880×32 baselines) using a bandwidth of 1 MHz for an integration time of 4 s.

Fig. 1.4: Variation of the system temperature and sensitivity (1σ) as a function of RA for the MRT survey. The minimum system temperature for an EW group is ≈650 K at RA≈04 hrs while the maximum system temperature is ≈2500 K at RA≈17:45 hrs. The minimum system temperature for an NS group is ≈660 K at RA≈04 hrs while the maximum system temperature is ≈2200 K at RA≈17:40 hrs. For the interferometer formed by the EW and the NS group, the minimum system temperature is ≈660 K at RA≈04 hrs and maximum system temperature is ≈2300 K at RA≈17:45 hrs. The minimum detectable sensitivity (including the confusion noise) is ≈111 mJy at RA≈04 hrs while the maximum sensitivity is ≈380 mJy at RA≈17:45 hrs.

The celestial sky consists of bright as well as faint sources. When a region of the sky is imaged with an instrument, there is always some probability that along with the source of interest that is the source above the desired flux density detection threshold, there are other unresolved fainter sources within the beam. These faint sources may be too weak to be perceived individually but collectively they limit the accuracy with which the measurements or estimation of the parameters of the source of interest can be ascertained. The uncertainty due to presence of unresolved fainter sources below the detection threshold affecting the estimation of the parameters of the source of interest, varies from one region to another that is one beam area to another. The variation of this uncertainty from one beam area to another is perceived in an image as a statistical fluctuation as if there was a real random noise in the image. This sets a limit below which it is not possible to decrease the system noise contribution in the image by increasing the integration time or observing bandwidth. This noise due to the statistical variation of the distribution of sources in the sky is called confusion noise.

The confusion noise due to unresolved sources depends upon only two factors. The first is the differential source counts at the frequency of interest around the detection threshold and the second is the resolution of the imaging instrument. The confusion noise increases as the resolution becomes poorer, as it increases the probability of finding an odd bright source in a broader beam. It is also important to note that the confusion noise does not cause uncertainty only in the determination of flux but also all other parameters like position, structure etc.. Assuming that the number of sources - flux density relation has a power law form,

$$n(S)\,dS = k\,S^{-\gamma}\,dS, \quad S > 0$$

where $n(S)$ is the number of sources per unit solid angle (Sr) per unit flux density interval (Jy). If we want to compute the total number of sources which are above a particular flux density say S_o(Jy), we need to integrate both the sides of the above equation.

$$N(>S_o) = \int_{S=S_o}^{S=\infty} kS^{-\gamma}\,dS = \frac{-k}{-\gamma+1}S^{-\gamma+1} \tag{1.4}$$

Here $N(>S_o)$ is the number of sources above the flux density S_o at the frequency under consideration. At 150 MHz, the number density of sources above 200 mJy is $\approx$20,000 Sr^{-1} (Baldwin et. al., 1985). Assuming a value of $\gamma = 2$ (based on source counts between 1 mJy and 1Jy at 1.4 GHz), we obtain the value k=4.0$\times$10^3 Jy$^{3/2}$ Sr^{-1}. The confusion noise is given by the expression (Condon, 1974),

$$\sigma_c = \left(\frac{q^3 - \gamma}{3 - \gamma}\right)^{\frac{1}{\gamma-1}} (k\Omega_e)^{\frac{1}{\gamma-1}} \tag{1.5}$$

where, σ_c is the confusion noise, q is a parameter of integration chosen as 3, Ω_e is the effective beam area, γ is the power law exponent of the flux density in the number-flux density relation, k is a constant which depends upon the differential source count. The effective beam area Ω_e, is given by (Condon, 1974),

$$\Omega_e = \frac{\pi}{4} \frac{\theta_1 \theta_2}{[(\gamma - 1)\ \ln 2]} \tag{1.6}$$

where θ_1 and θ_2 are the major and the minor axes of the telescope beam. Using the values of θ_1=4′, θ_2=4′(for the full resolution image), we get Ω_e=1.53×10^{-6} Sr. Substituting the values of k and Ω_e in the Eqn. 1.5, we obtain the value for the confusion noise, σ_c ≈18 mJy. Thus the confusion noise is far below the thermal noise (>110 mJy) in the MRT images.

In case of the survey with partial resolution (see Sec. 1.5.1), using θ_1=17′, θ_2=23′, we get Ω_e=3.52×10^{-5} Sr and the obtained value of the confusion noise σ_c ≈430 mJy.

c. **Total noise**

From Eqn. 1.2, knowing the thermal noise and the confusion noise we can calculate the effective value of minimum detectable point source sensitivity (ΔS_{min}). Fig. 1.4(b) shows the variation of the limiting point source sensitivity for the MRT as a function of RA. The minimum total noise is ≈111 mJy at RA≈04 hrs. The maximum total noise is ≈380 mJy at RA≈17:45 hrs. Thus the images from the MRT survey would be limited by thermal noise.

Surface brightness sensitivity: The expected point source sensitivity in the synthesized images in MRT is typically 110 mJy (1σ). The corresponding surface brightness sensitivity taking the resolution in the images as 4′×4′is given by,

$$B = \frac{S}{\Omega} = \frac{130 \times 10^{-29}}{(\frac{\pi}{4ln2})[\frac{4}{60} \times \frac{\pi}{180}]^2} \approx 7 \times 10^{-22}\ \mathrm{Wm^{-2}Hz^{-1}Sr^{-1}} \tag{1.7}$$

This is a good limit to investigate low surface brightness features in the radio galaxies and SNRs in our galaxy (see Sec. 7.4 for details).

Expected No. of sources: The expected number of sources in the MRT survey depends upon the minimum detectable point source sensitivity. Since we carry out meridian transit imaging, there is no attenuation in the flux density of a source due to the primary beam of the helix along Hour Angle (HA). However due to the primary beam of the helix in declination, the flux density of a source as apparent to the array would be the true flux density

attenuated by the response along declination, which will affect the detection threshold. The actual point source sensitivity, $S_{lim}(\delta)$ (which is considered as detection) at a declination δ, is given by,

$$S_{lim}(\delta) = \frac{S_o}{P(\delta)} \tag{1.8}$$

where S_o is the sensitivity at the declination where the primary beam response of the helix is maximum (at δ=-40°.14). Assuming a slope of log N-log S curve as -1.5, if the number density of sources above a flux density S_o be n_o, then the number density of sources which would be detected in the MRT images at a declination δ is given by,

$$n_{lim}(\delta) = \left(\frac{S_{lim}(\delta)}{S_o}\right)^{-\frac{3}{2}} n_o = P(\delta)^{\frac{3}{2}}\, n_o \tag{1.9}$$

Thus the total number of sources for a region ($N_{lim}\{(\phi_1,\phi_2),(\delta_1,\delta_2)\}$) between sidereal hour ϕ_1 and ϕ_2 and declination δ_1 and δ_2 is

$$N_{lim}\{(\phi_1,\phi_2),(\delta_1,\delta_2)\} = \int_{\phi 1}^{\phi 2}\int_{\delta_1}^{\delta_2} n_{lim}(\delta)\,\cos\delta\, d\delta\, d\phi = n_o\,(\phi_2-\phi_1)\int_{\delta_1}^{\delta_2}\cos(\delta)P(\delta)^{\frac{3}{2}}\, d\delta \tag{1.10}$$

The helix primary voltage pattern is given by Eqn. 1.16 and the power pattern is given by the square of the voltage pattern. At any declination δ the power response of the helix is given by (Kraus, 1988b),

$$P(\delta) = \left(\frac{\sin[\frac{\pi}{6}]\,\sin[3\frac{\psi(\delta)}{2}]\,\cos[\delta-\delta_{axis}]}{\sin[\frac{\psi(\delta)}{2}]}\right)^2 \tag{1.11}$$

where

$$\psi(\delta) = 2\pi\left(\frac{1.75}{6}\,\{1-\cos[\delta-\delta_{axis}]\}+\frac{1}{6}\right) \tag{1.12}$$

and δ_{axis} is the declination at which the helix axis is pointed. Substituting the value of P(δ) and carrying out the integration as given by Eqn. 1.10, we can estimate the number of sources expected in the MRT survey in terms of the source density expected in the direction of maximum response of the helix. This integral cannot be analytically solved. Numerical integration using *Mathematica*[16] between the declination range δ_1=-70° and δ_2=-10°gives,

$$N_{lim}\{(\phi_1,\phi_2),(-70^\circ,-10^\circ)\} = 0.560117\,\frac{(\phi_2-\phi_1)}{2\pi}\,n_o \tag{1.13}$$

For the entire sky covered $N_{lim}\{(0,2\pi),(-70^\circ,-10^\circ)\} = 3.51932\,n_o$. Therefore due to primary beam response of the helix along declination, MRT would be be able to detect about

[16]http://www.wolfram.com

S.No.	Source	L_ν (W Hz^{-1})	z_{lim}
1	FR I	10^{23}	0.01
2	FR I	10^{24}	0.035
3	FR I-FR II break	10^{25}	0.10
4	FR II	10^{26}	0.40
5	FR II	10^{27}	1.50

Table 1.3: Limiting redshift up to which sources of different luminosity can be detected in MRT survey (courtesy Somanah & Udaya Shankar (2002)).

73% of the sources which actually exist above the limiting point source sensitivity limit given by Eqn. 1.2.

The expected number density of sources above the flux density limit of 200 mJy is ≈20,000 Sr^{-1} (Baldwin et. al., 1985). Assuming the slope of the $\log N - \log S$ curve as -1.5 and using the Eqn. 1.2 and Eqn. 1.13 and the rms noise as shown in the Fig. 1.4(b), the total number of sources expected in the MRT survey is ≈36,800 for 3σ detection and ≈17,100 for 5σ detection.

Limiting redshift : The median redshift of the sources in the MRT survey would be ≈1 as discussed earlier. It is interesting to know the redshift limit up to which we can observe the radio sources of a given luminosity (Somanah & Udaya Shankar, 2002). The observed flux density ($S_\nu(\nu_{obs})$) is related to the actual luminosity ($L_\nu(\nu_{obs})$) of a source by the relation,

$$S_\nu(\nu_{obs}) = \frac{L_\nu(\nu_{obs})}{4\pi D^2 (1+z)^{1+\alpha}} \tag{1.14}$$

where $L_\nu \propto \nu^{-\alpha}$, taking Ω_o=1 and $D = \frac{2c}{H_o}\{1-(1+z)^{-1/2}\}$ (for $\wedge = 0$) (Scott et. al., 1994) we have,

$$\{z + 2(1 - \sqrt{1+z})\}(1+z)^\alpha = \frac{L_\nu(\nu_{obs})\, H_o^2}{16\pi c^2 S_\nu(\nu_{obs})} \tag{1.15}$$

Where z is redshift, H_o is Hubble constant, α is spectral index, c is speed of light and D is the effective distance. In the above Eqn. 1.15, we can find the limiting value of redshift (z) for a given value of luminosity. FR I sources[17] typically have their luminosity varying from 10^{23} to 10^{25} W Hz^{-1} whereas for FR II sources, the luminosity typically varies from 10^{25} to 10^{28} W Hz^{-1} (Fanaroff & Riley, 1974). Substituting $S_\nu(\nu_{obs})$=330 mJy (3σ) for MRT, we can calculate the limiting redshift for a radio source of a given luminosity (assuming a spectral index $\alpha = 0.7$). Table 1.3 shows the limiting redshifts for sources with different luminosities. The important point to note is that all the galaxies having luminosities more than 10^{27} W Hz^{-1} would be generally detected in the MRT survey, even if they are at high redshifts.

[17] based on Fanaroff & Riley classification.

Source Name	redshift (z)	S (Jy) at 365 MHz	S (Jy) at 151.5 MHz
8C 1435+63	4.25	2.823	5.224
6C 1014+326	4.41	0.451	0.834
4C 41.7	3.800	1.113	2.059
4C 60.7	3.790	1.120	2.072
MG 2144+192	3.594	1.730	3.201
4C 1243+036	3.581	1.947	3.603
B2 0902+34	3.395	1.129	2.089
B3 0744+464	2.926	1.851	3.425

Table 1.4: A few high redshift radio galaxies known in the literature and their flux density at 365 and 151.5 MHz (extrapolated assuming an spectral index of 0.7). The flux density of all the high redshift galaxies shown are above the minimum detection threshold of the MRT survey (330 mJy (3σ)).

Table1.4 shows some of the high redshift galaxies presently known along with their flux densities at 365 MHz and 151.5 MHz (extrapolating the flux assuming a spectral index of 0.7). As shown in the table, their flux densities are well above the minimum detectable sensitivity limit of MRT. From this we can infer that MRT sensitivity is good enough for us to look for a few new high redshift galaxy candidates.

It is also interesting to know the linear size of the sources at different redshifts which can be resolved by MRT. So we can ask the question : up to what redshift is a source of a given projected size resolved. Somanah & Udaya Shankar (2002) showed that sources of projected linear size more than 2 Mpc would be resolved in the MRT survey till redshifts of $\approx$1. So MRT survey should be able to resolve a few giant radio sources. They also showed that extragalactic radio sources with energy densities 2×10^{-14} Joules m^{-3} would get detected at MRT. Since energy densities in radio galaxies are typically of the order of 10^{-12} to 10^{-15} Joules m^{-3}, the MRT survey should also be able to detect most of the close ones.

1.5.3 The Mauritius Radio Telescope

The Mauritius Radio Telescope (MRT) (Golap et. al., 1998; Golap, 1998; Sachdev, 1999; Udaya Shankar et. al., 2002) is a Fourier synthesis array which has been constructed and operated collaboratively by the Raman Research Institute (RRI), Indian Institute of Astrophysics (IIA) and University of Mauritius (UOM). It is situated at Bras d'Eau (Latitude 20°.14 South, Longitude 57°.73 East) in the north-east of Mauritius, an island in the Indian Ocean. An aerial view of the MRT is shown in Fig. 1.5. It is a $\top$-shaped non-coplanar array with a 2048 m long EW arm having 1024 helices and a 880 m long NS arm having 15 movable trolleys with 4 helices each (see Ryle & Hewish (1960) for a general discussion about $\top$ arrays). The basic layout of the MRT is shown in Fig. 1.6. Important specifications of MRT are mentioned in Table 1.5.

Fig. 1.5: An aerial view of the Mauritius Radio Telescope. The non-coplanarity of the EW arm can be noticed. The observatory building is also seen.

Antenna System:

The basic element - Helix: The basic element of the antennae system is an axial mode helix shown in Fig. 1.7(a). The helices are mounted with a tilt of 20° towards the south so that they point towards a declination of -40°.14 at the meridian of transit. This tilt allows a better coverage of the southern sky including the southern-most part of the Galactic plane, a region largely unexplored at metre wavelengths. Due to circular polarization response of the helix, the observed source intensities are unaffected by Faraday rotation in the intervening medium including the local ionosphere. An approximate normalized far field voltage response ($V(\theta)$) in the direction of angle θ from the axis of the helix, for an axial mode helix is given by as (Kraus, 1988b),

$$V(\theta) = \frac{\sin(n\psi/2)}{\sin(\psi/2)} \sin\left(\frac{\pi}{2n}\right) \cos(\theta) \tag{1.16}$$

where n is the number of turns and $\psi = 2\pi[S_\lambda(1-\cos\theta) + (1/2n)]$, where S_λ is the spacing between the turns in units of wavelength. The theoretical voltage pattern and the power pattern ($V^2(\theta)$) of the MRT helix, as a function of angle with the helix axis is shown in Fig. 1.7(b). The helical antenna has a collecting area of λ^2 ($\approx$4 m^2 at 150 MHz) with a expected FWHM of about 56°.

The east-west arm: The east-west (EW) arm is 2048 m long having 1024 helices and divided into 32 groups. Due to the uneven rocky terrain these groups are not coplanar

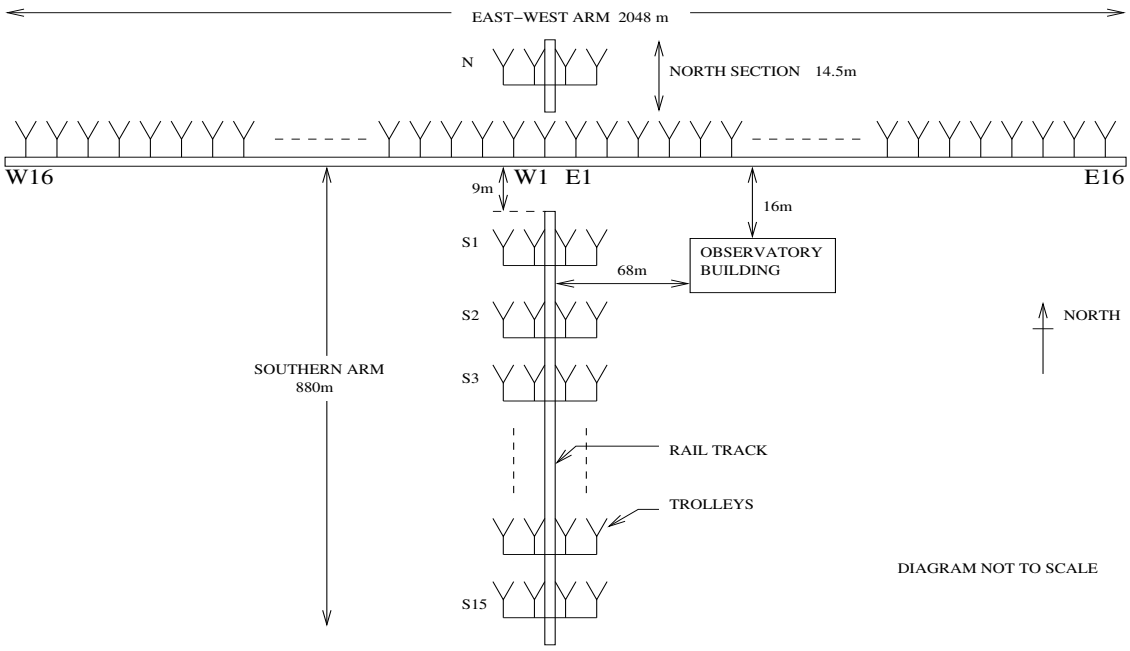

Fig. 1.6: A schematic of the MRT array. The EW arm has 1024 helices which are divided in 32 groups of 32 helices each. The NS arm has 15 movable trolleys each having 4 helices.

and have a maximum height difference of 35 m. Fig. 1.8(a) shows the height profile of the EW arm. The terrain was smoothed while constructing the array to ensure that antennas within each group are at the same height. The far-field primary beam power pattern of an EW group has a FWHM of about 2°×56° in RA and declination.

The north-south Arm : The north-south (NS) arm consists of 15 movable trolleys. The south track starts at a distance of 9 m from the EW arm and is about 880 m long. The closest that the helices on a trolley can get to the EW arm is 11 m due to the physical size of the trolleys. The south track has a downward slope of $\frac{1}{2}°$ till the 655 m mark and from there onwards it has an upward slope of 1°. Since the south arm cannot approach the EW array closer than 9 m, a north arm has been constructed which allows measurements down to 2 m spacing. The trolleys cannot approach closer than 2 m to the EW arm because of physical size of the trolleys itself. The north rail track is flat and 14.5 m long. The slope profile of the NS arm is shown in Fig. 1.8(b). The far-field primary beam power pattern of an NS group has a FWHM of about 15°×56° in RA and declination.

The Receiver System :

The front end of the receiver system has been built with sufficient bandwidth so that the observing frequency can be shifted (within 145-155 MHz) to an interference free zone by tuning the Local Oscillator (LO). The band around 151.5 MHz was found to be relatively quiet and has therefore been used. The details of the receiver system are available in

Location : Latitude	20.°14 S
: Longitude	57.°73 E
Observing frequency	151.5 MHz
Telescope configuration	$\top$ shaped array
Basic element	Helical Antenna
Polarization	Right Circular
Collecting area of a helix	4 m^2 at 150 MHz
FWHM of helix	56°
Declination coverage	-70° to -10°
East-west arm : length	2048 m
: composition	32 groups with 32 helices each
: collecting area	4096 m^2
North-south arm : length	880 m
: composition	16 trolleys, each with 4 helices
: collecting area	256 m^2
1^{st} IF frequency	30 MHz
2^{nd} IF frequency	10.1 MHz
Instrumental bandwidths (available)	0.15, 1.0, 1.5, 3.0 MHz
Digitization before correlation	2-bit 3-level, 1-bit 2-level
Correlation receiver	32×16 complex correlators
Number of baselines measured per day	32×16
Collecting area per baseline (1 EW×1 NS)	90 m^2
Sensitivity per baseline	26 Jy(τ=1 s, $\Delta\nu$ =1 MHz)
Minimum and maximum baselines	0, 661 λ
Self correlations	64
Minimum time required to get full resolution image	60 days
Synthesized beam-width	$4' \times 4.'6 \sec(\delta + 20.°14)$
Point source sensitivity	330 mJy ($3\,\sigma$; for T_{sys}=700 K; τ=4 s)

Table 1.5: Specifications of MRT.

Sachdev (1999); Golap et. al. (1998); Golap (1998). *Since for design purpose* 150 MHz *was used as the band center, we often refer to* 150 MHz *as the operating frequency although the actual frequency is* 151.5 MHz.

RF section : In each group in the EW, the four helices outputs are combined using a 4 way power combiner. The output is high-pass filtered and then amplified in the pre-filter amplifier unit. The noise temperature of the first amplifier is about 270 K. The total attenuation between the helix and the first pre-amplifier is about 1 dB (0.1 dB loss in the cable, 0.4 dB insertion loss in the 4-way combiner and 0.5 dB insertion loss in the pre-filter) and therefore the system temperature deteriorates[18] to about 400 K. Eight pre-filter amplifier unit outputs are further combined to produce a combined group output. In the NS group signal from the four helices on the trolley are combined similarly as in case of

[18]The noise temperature of the receiver-transmission line, T_{RT} is given by Kraus (1988a): $T_{RT} = (\frac{1}{\epsilon}-1)T_{LP}+\frac{1}{\epsilon}T_R$
Where ϵ is the transmission-efficiency coefficient, $0 \le \epsilon \le 1$. T_{LP} is the physical temperature of the transmission line. and T_R is the noise temperature of the receiver. For 1 dB attenuation, $\epsilon = \frac{1}{10^{\frac{1}{10}}} = 0.794$. Therefore, $T_{RT} = (\frac{1}{0.794} - 1) \times 290 + \frac{1}{0.794} \times 270 \approx 415$ K.

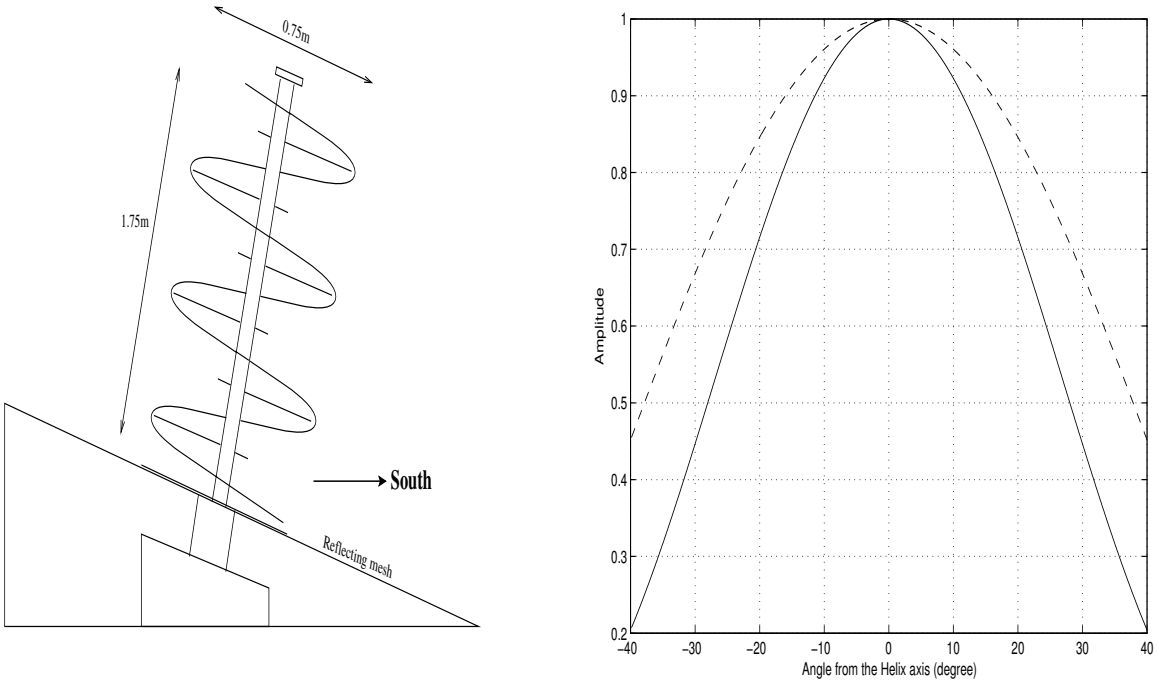

(a) A schematic of the MRT Helix: It is a peripherally fed monofilar axial mode helix of 3 turns with a diametre of 0.75 m and a height of 1.75 m. The helices are mounted with a tilt of 20° towards the south (Golap, 1998; Sachdev, 1999).

(b) The theoretical voltage pattern (dashed line) and the power pattern (solid line) of the helix as a function of angle form the axis of the helix in degrees. The FWHM of the power pattern is ≈56°.

Fig. 1.7: The basic element - Helix

EW group using a 4 way power combiner. The output is high pass filtered and amplified in a pre-filter amplifier unit. The system temperature is ≈400 K. In total, the entire RF section consists of 272 low noise amplifiers.

IF section : The EW group output is heterodyned to 30 MHz using an Local Oscillator of 121.5 MHz. Heliax cables running parallel to the east, west and south arms of the array are used to distribute the LO signal required for heterodyning. The heterodyned signal is then passed through a bandpass filter centered at 30 MHz and amplified. The output is transmitted to the observatory via a 1050 m coaxial cable in the eastern arm and a 1100 m coaxial cable in the western arm. Approximately equal lengths of cables have been used for all the groups irrespective of their distance from the observatory. This ensures similar phase variations in all the groups due to change in the ambient temperature. The NS group output is sent to the mixer unit where it is processed in the same way as in an EW group and is then transmitted to the observatory using a coaxial cable of about 1000 m. Depending on the distance from the center of the south arm, a part of these IF cables are rolled on to a spool attached to the trolley.

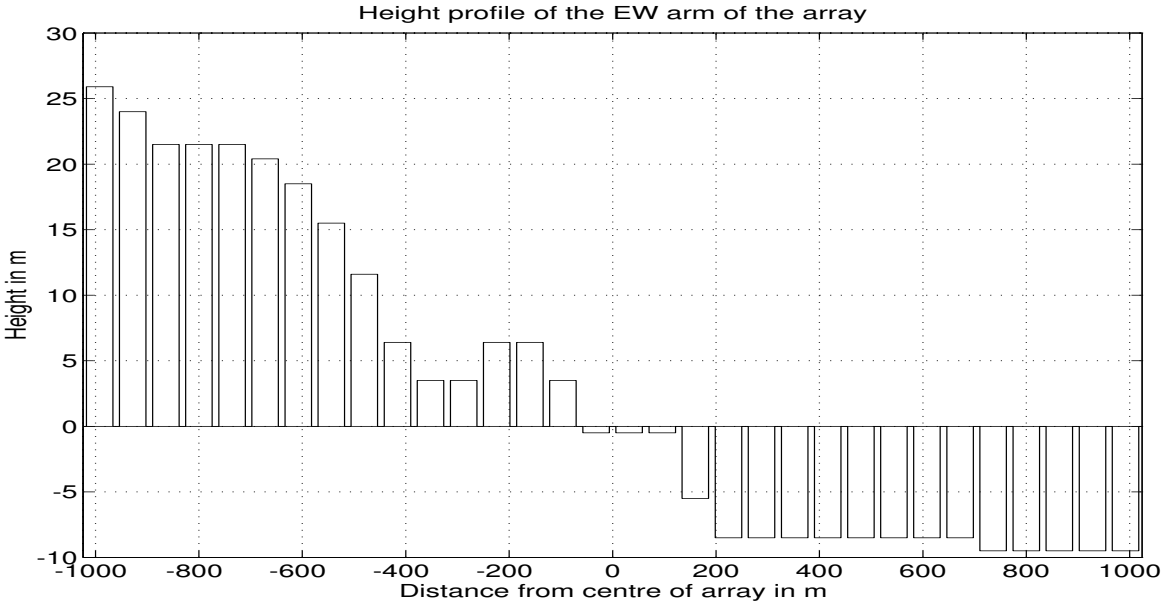

(a) The EW height profile : The heights of the 32 EW groups as a function of their distance from the centre of the array. Due to the uneven terrain, they are not at the same height and the maximum height difference in the EW arm is 35 m.

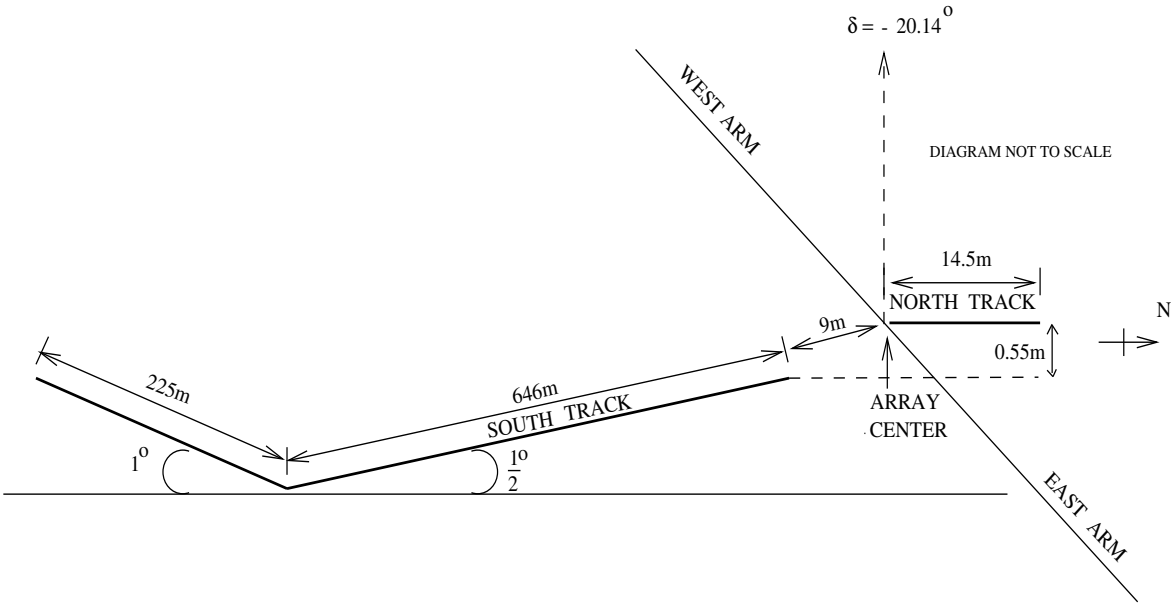

(b) NS slope profile: The south track has a downward slope of $\frac{1}{2}^\circ$ till about the 655 m and from there onwards it has an upward slope of 1°. The north track is flat.

Fig. 1.8: The profile of the EW and the NS arm of the MRT array.

The signals from the EW and the NS groups are brought separately to the observatory building via coaxial cables. In the observatory, the last group of the east array (E16) is split in two for use in calibration. The 48 channels (32 EW, 15NS, E16) are split using a hybrid with one output of each hybrid sent to a monitor port and the other output, to the second mixer unit, via a bandpass filter centered at 30 MHz. The signal is further amplified before being heterodyned using passive mixers and an LO of 40 MHz. The mixer output is then filtered by bandpass filters centered at 10.1 MHz. Four selectable filters of bandwidths 0.15 MHz, 1 MHz, 1.5 MHz and 3.0 MHz are available. The filtered outputs go through an *Automatic Gain Control* (AGC) unit, which keeps the signal level constant to the samplers.

Sampler : The second-IF outputs of the 32 EW and 16 NS (15NS and E16) groups are fed to a broadband quadrature hybrid which splits the signal into quadrature phase channels – the in-phase (cos) and the quadrature-phase (sin) channel outputs. These two channels are then amplified to produce a signal with an rms of 1 V. The cos and the sin channels are then quantized by comparators with threshold voltages (V_{th}) of about ±0.7 V producing 3-level amplitude quantization. After the comparators, the quantized signal is sampled in subsequent flip-flops (F/F) at the rate of the correlator clock frequency, which can be up to 12 MHz. These are then processed in a 2-bit 3-level correlator. In a 2-bit 3-level correlator sampling the digitized signal at Nyquist rate, the maximum sensitivity obtainable relative to an analog correlator is 0.81. This is obtained when V_{th}/σ is 0.61. The sensitivity changes only by ≈5% from this optimal value when the signal power changes by 40% (Bower & Klinger, 1974).

Correlator and Recirculator system : The digitized data is sent to the correlator boards via the delay boards. The correlation receiver provides 512 complex correlators, wherein 32 channels are cross-correlated with 16 channels. Although the use of larger bandwidth results in better sensitivity of a telescope, it restricts the angular range over which an image can be made if the relative delays between the signals being correlated are not compensated. When the uncompensated delay between the signals becomes comparable to the inverse of the bandwidth, the signals will be decorrelated. At MRT we use a bandwidth of 1 MHz. Since the EW group has a narrow primary beam of 2° in RA, this bandwidth does not pose a problem for synthesizing the primary beam in this direction. However, both the EW and the NS groups have wide primary beams in declination extending from -70° to -10°. So we need to compensate geometric delays for zenith angles along declination on the meridian. The correlation response around the direction of delay center for which the delay is compensated is then graded by $\frac{\sin(\pi\,\Delta\nu\Delta\tau)}{(\pi\,\Delta\nu\Delta\tau)}$ where $\Delta\tau$ is the uncompensated delay in any other declination. In order to keep the effect of bandwidth decorrelation to less than 20% even on the longest baselines (along NS) in the entire declination range -70°≤ δ ≤-10°, the

visibilities are measured with four different delay settings. For each delay setting a small part of the sky in declination can be observed without appreciable decorrelation, which is referred as a delay zone. A recirculator system was designed and built which allows observations with different delay settings in one observation schedule using the available correlaor system (Sachdev & Udaya Shankar, 2001a). In this system, the data is sampled at a rate of 2.65625 MHz, stored in a buffer memory and the correlations are measured at four times this rate (10.625 MHz). Such a processing by the correlator at a higher speed than the input rate allows the correlations to be measured with four delay settings. The loss of sensitivity due to reduction in the sampling rate for a 1 MHz bandwidth, from 12 MHz to 2.65625 MHz for a 2-bit 3-level correlator is only about 10%.

Self correlators : Sixty four self-correlators are also provided wherein each channel is correlated with itself with zero delay. The self-correlators of the MRT are wired such that they measure the probability (P), that the input signal amplitude V, is in between the threshold levels used for digitization. This probability for a zero-mean Gaussian signal with RMS fluctuation of σ and a symmetric 2-level digitizer with voltage threshold levels $\pm V_{th}$, is given by,

$$P = \frac{1}{\sigma\sqrt{2\pi}} \int_{-V_{th}}^{+V_{th}} e^{-(\frac{V}{\sqrt{2}\sigma})^2} dV = \mathrm{erf}(\frac{V_{th}}{\sqrt{2}\sigma}) \tag{1.17}$$

Knowing P, the $\frac{v_{th}}{\sigma}$ of the signal can be obtained. This provides the necessary information for obtaining the normalized correlation coefficient ρ, from the measured digital correlation counts (Addario et. al., 1984).

$$\rho = \gamma - \frac{\gamma^3(\alpha_1^2 - 1)(\alpha_2^2 - 1)}{6} \tag{1.18}$$

where $\gamma = (\pi/2)(N/N_{\max})e^{(\alpha_1^2+\alpha_2^2)/2}$. α_1 and α_2 are the V_{th}/σ of the two channels being correlated and $N/N_{\max}$ is the ratio of correlation counts to the maximum possible value in a 2-bit 3-level system.

The AGCs maintain a constant signal level to the samplers even though the brightness distribution of the sky changes as the sky drifts through the meridian. This results in similar correlations for a weak source in a weak background and for a strong source in a correspondingly stronger background. Therefore we do not get the amplitude information of the signal from the sky. To recover the amplitude information while using the AGC, there is a need to keep track of the gains. In many telescopes this is done by adding a fixed amount of a known signal at each antenna. At MRT, however, the variation in the background radiation as seen by the EW and the NS groups are measured separately by switching off the AGC, in one EW and NS groups using the self-correlators to measure the total power output

of these groups. Since the EW and the NS groups have very broad beams, the power output of these groups does not change much (< 3dB) in the 24 hour period. This results in the variation of signal to noise ratio over the 24 hour cycle to be less than 5%. The equivalent analog correlation, ρ_a, is then obtained using the relation

$$\rho_a = \rho \times \sigma_1 \times \sigma_2 \tag{1.19}$$

where σ_1 and σ_2 are the RMS of the signals correlated. σ_1 and σ_2 are obtained from the channels where the AGCs have been switched off.

Data Acquisition and Control System (DAS) : DAS was designed and built to program the correlator system, recirculator boards and to acquire data from the correlators. At the end of each integration period (≈1.1 s) the data packets comprising of 512 complex visibilities, 64 self correlation measurements, 4 non-AGC self correlation measurements and sidereal time read from the astronomical clock are transferred to the hard drive for each delay zone separately. To facilitate data handling and automation of data processing, the data is organized in hourly Local Sidereal Time (LST) files. The allocation, the LST hour and the Julian Day (JD) information of the observation are directly obtainable from the name of the observation file. More details are given in Sachdev (1999).

1.6 Thesis layout

The thesis is organized in the form of eight chapters including the present one and two appendices. In the next chapter we first briefly summarize the observations for the survey (prior to this thesis work) and describe the organization of the resulting dataset. The data analysis software system developed to provide various new functionalities is briefly described along with the substantial improvements implemented on the existing software system. Chapter 3 presents a novel framework developed for automatically evaluating quality of astronomical data for the survey, its implementation, results and possible applications. Chapter 4 discusses a hierarchical RFI mitigation system developed and implemented on MRT data and also describes interference statistics. Chapter 5 describes the various aspects of wide field imaging with MRT, making of dirty images and techniques developed for image analysis. Chapter 6 discusses deconvolution of wide field images made with the non-coplanar MRT array, the algorithm developed, its implementation and results. Chapter 7 presents consolidated results in the form of deconvolved images covering more than a steradian of the sky as contour maps. The procedure developed for flux calibration involving scaling different images to a common level, estimation of the primary beam shape of the helix and recovery of the amplitude information of the signal lost in a

2 bit - 3 level correlator with an AGC are discussed. Important properties and a few interesting aspects of the images are also discussed, including a few of the interesting sources in the images. An algorithm developed for construction of the source catalogue from the wide field deconvolved images is also described. The resulting source catalogue of nearly 2,800 sources derived from the images is presented in Appendix B. Appendix A presents dirty images covering an additional ≈0.5 steradian of the sky which includes a large part of the Galactic plane. Chapter 8 summarizes the results and discusses some interesting likely future directions for our work.